



UNIVERSITY OF LEEDS

This is a repository copy of *Influence of Ni/SiO<sub>2</sub> catalyst preparation methods on hydrogen production from the pyrolysis/reforming of refuse derived fuel*.

White Rose Research Online URL for this paper:  
<http://eprints.whiterose.ac.uk/80743/>

Version: Accepted Version

---

**Article:**

Blanco, PH, Wu, C and Williams, PT (2014) Influence of Ni/SiO<sub>2</sub> catalyst preparation methods on hydrogen production from the pyrolysis/reforming of refuse derived fuel. *International Journal of Hydrogen Energy*, 39 (11). 5723 - 5732. ISSN 0360-3199

<https://doi.org/10.1016/j.ijhydene.2014.01.150>

---

**Reuse**

Unless indicated otherwise, fulltext items are protected by copyright with all rights reserved. The copyright exception in section 29 of the Copyright, Designs and Patents Act 1988 allows the making of a single copy solely for the purpose of non-commercial research or private study within the limits of fair dealing. The publisher or other rights-holder may allow further reproduction and re-use of this version - refer to the White Rose Research Online record for this item. Where records identify the publisher as the copyright holder, users can verify any specific terms of use on the publisher's website.

**Takedown**

If you consider content in White Rose Research Online to be in breach of UK law, please notify us by emailing [eprints@whiterose.ac.uk](mailto:eprints@whiterose.ac.uk) including the URL of the record and the reason for the withdrawal request.



[eprints@whiterose.ac.uk](mailto:eprints@whiterose.ac.uk)  
<https://eprints.whiterose.ac.uk/>

## **Influence of Ni/SiO<sub>2</sub> catalyst preparation methods on hydrogen production from the pyrolysis/reforming of refuse derived fuel**

Paula H. Blanco, Chunfei Wu, Paul T. Williams\*

Energy Research Institute, University of Leeds, Leeds, LS2 9JT, UK

(Tel: #44 1133432504; \*Email: p.t.williams@leeds.ac.uk)

**ABSTRACT:** Hydrogen production from the pyrolysis/reforming of refuse derived fuel (RDF) was investigated with a series of Ni/SiO<sub>2</sub> catalysts. The catalysts were prepared by homogeneous precipitation derived from a sol-gel method (HPG) and compared to Ni/SiO<sub>2</sub> catalysts prepared by adding a phase separation step to the HPG process (B-HPG). All the catalysts had a NiO loading of 10 wt.%, and three different calcination temperatures (500 °C, 700 °C and 900 °C) were used for each method. The prepared Ni/SiO<sub>2</sub> catalysts were analysed to determine their surface area, and porosity characteristics; additionally scanning electron microscopy (SEM-EDX), transmission electron microscopy (TEM), infrared spectroscopy (FTIR), and X-Ray diffraction (XRD) analyses were carried out. The results showed that the catalyst prepared by HPG and calcined at 700 °C (HPG700), presented a relatively high surface area (~347 m<sup>2</sup>g<sup>-1</sup>), large pore diameter (12.50 nm), and also resulted in the highest catalytic activity towards H<sub>2</sub> production, attaining ~60 vol.% hydrogen. The lowest hydrogen concentration of about 42 vol.% was obtained using the catalysts prepared by the combined HPG-phase separation method, and calcined at 900 °C (B-HPG900). It was also observed that at calcination temperatures higher than 700 °C the catalytic activity for hydrogen production was diminished for both preparation methods.

**Keywords:** Sol-gel; Pyrolysis; Reforming; Gasification; RDF; Nickel catalyst

## 1. Introduction

The use of hydrogen as an alternative fuel has attracted attention for applications in processes such as internal combustion engines, fuel cells or turbines for power generation. Currently, about 90% of world hydrogen production is based on reforming of natural gas, and other fossil fuels, involving CO<sub>2</sub> generation [1,2]. Waste-to-energy applications including thermal treatments such as pyrolysis and gasification involves the generation of a hydrogen rich syngas, and are a viable option when seeking a clean and sustainable energy production cycle [2]. The resulting gas contains other components such as CO, CO<sub>2</sub>, O<sub>2</sub>, CH<sub>4</sub>, C<sub>2</sub>-C<sub>4</sub>, together with some particulate matter and also some organic and inorganic impurities identified as tar.

Different techniques have been studied in relation to gas cleaning, including physical, mechanical, catalytic and thermal cracking methods. Catalytic steam reforming has been widely used in industry as it promotes tar cracking reactions and also increases the hydrogen concentration in the produced gas. Different types of catalysts have been prepared, characterised and tested within different processes, particularly including research on nickel based catalysts due to their industrial relevance [3]. For example Ni catalysts have been used during steam reforming processes due to their outstanding reactivity, hydrogen selectivity, and low cost compared with other metals such as Rh or Pt [4,5]. Additionally in order to increase the catalytic activity and performance, some features of the catalyst such as pore size, surface area and metal dispersion have been modified through the use of different types of supports and preparation methods [6-8].

For example Ni/SiO<sub>2</sub> catalysts prepared by conventional impregnation or ion exchange processes have been reported to produce low surface area and also to present problems associated with poor Ni dispersion that might result in catalyst deactivation, as at high Ni loadings the fine Ni particles tend to aggregate during calcination and further reduction [5]. On the other hand, Ni/SiO<sub>2</sub> catalysts prepared by sol-gel methods reported a better

performance when compared with catalysts prepared by conventional impregnation during the CO<sub>2</sub> reforming of methane [9]. Advances in sol-gel methods have been restrained due to the complexity in producing well dispersed metal particles (<10nm), especially at metal loadings higher than 15wt.%, achieved using a metal salt as the catalyst precursor [10]. One of the solutions to solve this problem has been the use of dispersed hydroxide (or oxide), and tetraethoxysilane (TEOS) in an acidic medium as metal and SiO<sub>2</sub> precursors respectively during the preparation process [10]. In this way, the reaction between TEOS and nickel nitrate promotes higher metal dispersion, in addition, higher surface area might be obtained compared with other oxide supports such as alumina oxide and titanium oxide [9,11]. Furthermore an improved sintering resistance of the final catalyst and a reduction in the catalyst deactivation might be attained [12,13]. It has been also reported that the thermal stability and porous properties of nickel based catalysts might be also improved using silica oxide as a catalyst support [9,14,15].

There are several sol-gel methods for catalyst preparation. For example, a preparation method known as homogeneous precipitation (HPG), has been used to promote the metal dispersion inside the porous silica matrix, thus the resulting catalyst possesses high thermal stability, and high sintering resistance as the Ni metal particles are entrapped within a silica network (preparation method pathway from Supplementary Figure S1(a)) [15-17]. Furthermore, Takahashi and collaborators [18], suggested the addition of a phase separation step after the homogenous precipitation; resulting in a catalyst containing both macropores and mesopores. It was found that by combining both the phase separation and the gelation process, the distribution of pores in the catalyst was greatly affected (see Supplementary Figure S1(b)).

In this work, a series of six different Ni/SiO<sub>2</sub> catalysts was prepared using two different methods with the additional of varying the calcination temperature (500 °C, 700 °C and 900

°C). The catalysts were tested for hydrogen production in a two-stage pyrolysis/reforming reaction system, using municipal solid waste in the form of refuse derived fuel (RDF) as the raw feedstock material. The relationships of catalytic performance in terms of hydrogen production and their structural properties e.g. surface area have also been investigated.

## 2. Methodology

### 2.1 Materials and sample preparation

Refuse Derived Fuel (RDF) from Municipal Solid Waste was used as the raw feedstock material with a particle size of ~1.0 mm. The composition of the RDF was 43wt.% of carbon, 6wt.% of hydrogen, 32wt.% oxygen and 0.5wt.% of nitrogen. In addition, the proximate analysis of the RDF was 7% moisture content, 15% of ash content and 67% of volatile matter. Six different Ni/SiO<sub>2</sub> catalysts with 10 wt.% of NiO concentration were prepared by two different methods. The preparation methodology was adapted from the literature for homogeneous precipitation in wet gel (HPG) [15], and combined phase separation and HPG methods [18]. For the HPG method, tetraethoxysilane (TEOS) and nickel nitrate hexahydrate (Ni(NO<sub>3</sub>)<sub>2</sub>·6H<sub>2</sub>O) both from Sigma-Aldrich, were used as sources of silica and nickel respectively. Nitric acid (HNO<sub>3</sub>; ARISTAR), and urea (CH<sub>4</sub>N<sub>2</sub>O; analytical/reagent grade Fisher Scientific) were also used as raw materials. The initial composition used was TEOS: 0.1mol dm<sup>-3</sup> HNO<sub>3</sub> aq: Ni(NO<sub>3</sub>)<sub>2</sub>·6H<sub>2</sub>O: urea = 18.7: 20.0: 2.34: 4.09 in wt.% to obtain the final concentration of 10wt.% NiO. Nickel nitrate and urea were added into an aqueous solution 0.1mol dm<sup>-3</sup> of HNO<sub>3</sub>; then TEOS was dropped into the solution that became homogeneous after constant stirring, as ethanol and silanol were formed and acted as homogenizing agents, promoting the hydrolysis of silanes [19]. The homogeneous solution

was placed into an open container at 20 °C until it became a wet gel; the wet gel was then kept in a sealed container at 50 °C for one day. After that the temperature was increased up to 80 °C; and the gel was kept at constant temperature for 7 days for aging and to promote the urea decomposition. The obtained dry gel was further dried at 80 °C for 5 more days. The dried gel was calcined for 3 hours under air atmosphere at three different temperatures 500 °C, 700 °C and 900 °C; the calcined homogeneous precipitated catalysts were assigned as HPG500, HPG700 and HPG900.

For the combined phase separation and HPG method, the preparation method was based on that reported by Tomiyama et al [18]. For this procedure the same raw materials were used together with polyethylene oxide (PEO; ACROS Organics), deionised water and a 60wt.% aqueous solution of nitric acid (HNO<sub>3</sub>; ARISTAR). PEO was used as polymer additive as it has been reported to act as a template, controlling the morphology of macropores [11,16]. The initial composition was fixed at TEOS: Ni(NO<sub>3</sub>)<sub>2</sub>·6H<sub>2</sub>O: PEO: urea: H<sub>2</sub>O: 60wt.% HNO<sub>3</sub> aq. Corresponding to 26.6: 3.7: 3.2: 4.0: 32.0: 2.8 in weight ratio to obtain a final concentration of 10wt.% NiO. PEO, urea and nitric acid were initially dissolved into the nitric acid aqueous solution mixed with water, and then TEOS was dropped into the solution with continuous stirring until it became a homogeneous solution. The homogeneous solution was kept in a sealed container at 50 °C for 20 hours for gelation and phase separation; the resulting wet-gel was further aged at 80 °C for 7 days to promote urea decomposition and increasing in this way the pH of the solution due to ammonia formation. One of the most important variables to be controlled during the catalysts preparation was the pH, as in this particular case an increase in the pH promotes a ripening of the silica network and a homogeneous deposition of nickel hydroxide [18]. The dried gel was then further dried at 80 °C, and then the composite was calcined at three different calcination temperatures 500 °C, 700 °C and 900 °C for 3 hours; the prepared catalysts were assigned as B-HPG500, B-

HPG700 and B-HPG900; where B refers to the bimodal combined phase separation and HPG method, and their respective calcination temperatures. All the prepared catalysts were crushed and sieved to obtain granules between 0.05-0.18 mm particle sizes. All the experiments were repeated to ensure reliability and reproducibility.

## 2.2 Pyrolysis/reforming reaction system.

The Ni/SiO<sub>2</sub> catalysts were tested under the same pyrolysis/reforming conditions, using RDF as raw material; with a catalyst:RDF ratio of 1:2. The experimental details have been described elsewhere [20-22]; however a brief description is as follows. A two-stage pyrolysis/reforming reactor was used; the pyrolysis temperature was set at 600 °C whereas the reforming stage was carried out at 800 °C. Two thermocouples located in each reactor of the two stage reactor system were used to control the temperatures. The reforming temperature was set at 800 °C to promote the catalyst activation. Once the reforming temperature was reached, the pyrolysis temperature was increased up to 600 °C, the decomposition of RDF has been reported to start at 230 °C [23]. At the same time, water as steam was introduced with a flow rate of 5ml h<sup>-1</sup> and mixed with the evolved RDF pyrolysis gases. The gases mixture was passed through the second reforming stage using nitrogen as carrier gas. The produced gases after reaction were passed through a cooling system consisting of two condensers cooled by air and dry-ice respectively, the condensed fraction was collected within both condensers; and the non-condensed gases were collected in a gas sample bag for further analysis.

The produced gases were analysed by gas chromatography (GC) to determine hydrocarbons (CH<sub>4</sub>, C<sub>2</sub>-C<sub>4</sub>) and permanent gas concentrations (H<sub>2</sub>, CO, N<sub>2</sub>, O<sub>2</sub>, CO<sub>2</sub>); the GC

analysis details are reported elsewhere [20]. The experiments were repeated at least three times to check reliability.

### 2.3. Catalysts characterization.

Nitrogen adsorption-desorption isotherms of fresh Ni/SiO<sub>2</sub> samples were measured at -196 °C using a BET Quantachrome NOVA 2200e series apparatus. Each sample was previously degassed at 120 °C for 3 hours under vacuum prior to measurement. The specific surface area was calculated from the adsorption curve according to the Brunauer-Emmet-Teller (BET) method [24]. Micropore and mesopore distributions were obtained using the Dubinin-Radushkevich (DR) method, whereas the pore diameter was calculated according to the Barrett, Joyner and Halenda (BJH) method [25]. The pore size distributions were calculated using the regularization method according to the Density Functional Theory (DFT), based on a molecular model of nitrogen adsorption in porous solids [26]. This method is useful to characterize adsorbents according to their porous structure and surface properties, from experimental adsorption isotherms [27].

A high-resolution scanning electron microscope (SEM, LEO 1530) coupled to an energy dispersive X-ray spectroscope (EDXS), were used to obtain images of the morphology of fresh and reacted Ni/SiO<sub>2</sub> catalysts. Selected catalyst samples (fresh and reacted), were dispersed in ethanol to be observed by transmission electron microscopy (TEM, Phillips CM200). A Bruker D-8 diffractometer was used to record the XRD patterns of the prepared catalysts using a Cu-K $\alpha$  X-ray source with a Vantec position sensitive detector; corundum was used as an external standard. Nickel crystallite size was determined according to Scherrer's method from the broadening of the line. Fourier transform infrared spectroscopy (FTIR) was also used to verify the composition of fresh catalysts [20]. The FTIR analyses

were carried out using a Thermo Nicolet Scientific spectrometer (iS10); the FTIR plate was cleaned with acetone before each analysis, a small amount of each catalyst was placed onto the plate. In order to detect residual carbons in the reacted catalysts, temperature programmed oxidation and their derivative curves (TPO-DTG) were obtained using a Stanton-Redcroft thermogravimetric analyser (TGA). About 20 mg of each reacted catalyst were placed in a sample pan and heated up to 800 °C with 15 °C min<sup>-1</sup> heating rate, and 10 minutes holding time. Temperature programmed reduction (TPR) was carried out to characterize the selected fresh catalysts using a Stanton-Redcroft thermogravimetric analyzer (TGA). During the TPR analysis, the fresh catalyst was heated at 20 °C min<sup>-1</sup> to 150 °C and held for 30 min under the atmosphere of hydrogen (5% H<sub>2</sub> balanced with N<sub>2</sub>), then heated at 10 °C min<sup>-1</sup> to 900 °C with a flow rate of 50 ml min<sup>-1</sup>.

### **3. Results and Discussion**

#### **3.1 Characterisation of fresh catalysts**

The BET surface area and porous characteristics of the prepared Ni/SiO<sub>2</sub> catalysts are presented in Table 1. From Table 1, for the series of catalysts prepared by the HPG method, the surface area was reduced, as the calcination temperature was increased from 500 °C to 900 °C. This trend is consistent with data reported previously by Tomiyama and co-workers [15]; they prepared Ni/SiO<sub>2</sub> catalysts by homogeneous precipitation in wet gel (HPG) varying the calcination temperature, and observed a gradual decrease in the specific surface area of the Ni/SiO<sub>2</sub> catalysts as the calcination temperature was increased from 500 °C up to 1000 °C. This decrease might be related with reduction forming interphase silica-like compounds formed by increasing the calcination temperature [28]. However, the surface area for the

catalysts prepared by the combined B-HPG method seemed to be increased with the increase of the calcination temperature from 500 to 700 °C; and reduced at 900 °C calcination temperature. A similar effect in relation to the surface area was observed by Takahashi et al. [18], while increasing the calcination temperature from 500 °C up to 700 °C during the preparation of Ni/SiO<sub>2</sub> catalysts by a similar method using a 20 wt.% Ni loading.

N<sub>2</sub> adsorption-desorption isotherms of the fresh catalysts are shown in Figure 1. It was observed that the isotherm trend for Ni/SiO<sub>2</sub> catalysts prepared by a conventional homogeneous precipitation method (HPG) was a type V isotherm (Figure S2) [29]. These types of isotherms are uncommon and are related with weak adsorbent–adsorbate interactions for mesoporous materials. Additionally the sharp inflection in the P/P<sub>0</sub> range from 0.70 to 0.90, it is usually related to capillary condensation and evaporation processes within uniform pores. The hysteresis loop is of the H1 type associated with porous materials consisting of agglomerates or compacts of uniform sphere arrays, also presenting a narrow distribution of pore size. Hysteresis loops of type H1 have been observed on mesoporous silica with a regular array of cylindrical pores and predetermined diameters such as MCM-41 [30] and SBA-15 [31].

Additionally, from Figure 2(a), a narrow pore size distribution with average pore size around 7.5nm could be observed for the HPG500 and HPG900 catalysts; however the distribution of the HPG700 catalyst showed a shift in the pore distribution resulting in an average diameter of around 9nm. For the HPG900 catalyst, the mesopore volume, pore diameter (Table 1), and the average pore size are all smaller compared with the HPG700 and HPG500 catalysts (Figure 2(a)) which might suggest shrinkage in the pores during the calcination process [15].

The isotherms of the catalysts prepared by bimodal homogeneous precipitation and phase separation (B-HPG) methods (Figure 1), were also of type V; however unlike the

catalysts prepared by the simple HPG method, the hysteresis loop was of the H3 type (Figure 1), generally found in solids with a wide pore size distribution (Figure 2(b)) and by adsorbents with slit-shaped pores. Also the hysteresis loop closes until the equilibrium pressure or very close to the saturation pressure [32]. From Figure 2(b) it is observed that the B-HPG catalysts presented polydisperse distribution. Variations in pore size distribution are attributed to the velocity at which the phase separation and gelation process took place, followed by aging in a basic solution resulting in a bi-continuous structure with larger pores within the silica skeleton. Normally the pores are formed during the fixation of transitional structures of spinodal decomposition in the sol-gel transition of inorganic components [18].

In Figure 3, XRD (Figure 3(a)) patterns and IR spectra (Figure 3(b)) are presented for selected HPG and BHPG Ni/SiO<sub>2</sub> catalysts. From the XRD analysis (Figure 3(a)), it is observed that all the samples exhibited a broad peak at around 22°, generally related with amorphous silica, and associated with a low degree of crystallization of the silica support [33]. This effect was also observed within the IR spectra (Figure 3(b)). The absorption band identified around 1060cm<sup>-1</sup> highlights the presence of Si-O-Ni bonds; it has been reported that originally this band is observed at around 1100cm<sup>-1</sup> and the shift of this absorption band from 1100 to 1060cm<sup>-1</sup> has been attributed to the formation of poorly crystalline 1:1 phyllosilicate of the nepouite type [28].

The diffraction peaks observed around 36°, 43° and 62°, were related to the presence of the Ni oxide crystals NiO(101), NiO(012), and NiO(110), respectively [34]. It has been reported in the literature that these characteristic NiO peaks tend to become more defined with the increase of the calcination temperature, for HPG and impregnated Ni/SiO<sub>2</sub> catalysts [15,35]. However from Figure 3(a), no noteworthy changes were apparent. On the other hand, when comparing these diffraction peaks for the HPG and BHPG catalysts (36°, 43° and 62°), it was observed that for the HPG samples the diffraction peaks were smaller and broader;

which might indicate that the particle size of NiO is smaller for the HPG samples [18]. The crystallite sizes estimated from the full width at half maximum of the diffraction peak using Scherrer's equation were 2-4 nm for the HPG samples and 3-5 nm for B-HPG catalysts. Regarding the Si-O interactions, from the IR spectra (Figure 3(b)) the two absorption bands identified around  $1060\text{cm}^{-1}$  and  $790\text{cm}^{-1}$  have been previously attributed to asymmetrical and symmetrical stretching motions of the silica skeleton of the type Si-O respectively [28].

From the TEM analysis of fresh catalysts (Figure 4(c) and 4(d)), the many dark spheres correspond to individual nickel particles distributed throughout the silica lattice. Similar morphologies have been previously reported for Ni/SiO<sub>2</sub> catalyst systems analysed by TEM [6,10,15,28]. For the HPG700 catalyst (Figure 4(c)) it was observed that most of the nickel particles are distributed through the silica matrix, whereas for the B-HPG700 catalyst (Figure 4(d)) a more homogenous metal dispersion was observed; that might be attributed to a broader pore size distribution (Figure 2(b)), attained by the induction of the phase separation step after the sol-gel transition during catalyst preparation.

Selected TPR results are shown in Figure 5. The main reduction of the fresh catalyst appears to occur at around 780 °C, indicating a strong interaction between the metals and the support. In addition, catalysts prepared at a higher calcination temperature (900 °C) demonstrated higher reduction temperature compared with catalyst calcined at 700 °C. In particular, the HPG 700 catalyst exhibited other weak reduction peaks at temperatures around 550 and 650 °C, indicating the presence of Ni-species having a lower interaction with the support compared with other catalysts.

### 3.2. Catalytic activity of the Ni/SiO<sub>2</sub> catalysts during pyrolysis/reforming of RDF.

The produced gases from the pyrolysis/reforming of RDF were analysed by gas chromatography and the gas composition was calculated on a nitrogen free basis. Table 2 shows the concentration of permanent gases and light hydrocarbons, product yields, and mass balance obtained for all the experiments. The gas yield was calculated considering the final weight of produced gas divided by the initial weight of the sample (RDF); additionally the hydrogen production was obtained calculating the mmol of hydrogen contained in the final gas mixture and divided by the initial RDF weight.

For the Ni/SiO<sub>2</sub> catalysts prepared by the HPG method, the highest activity towards hydrogen production attained was 21.5 mmol H<sub>2</sub> g<sup>-1</sup><sub>RDF</sub> using the HPG700 catalyst, which at the same time resulted in the lowest CH<sub>4</sub> and C<sub>2</sub>-C<sub>4</sub> gas concentrations. Additionally a lower CO<sub>2</sub> concentration was attained using this catalyst, which might indicate a greater promotion of steam reforming reactions and a reduced promotion of the water-gas shift reaction, when compared with the other two HPG catalysts (Table 2). TPR results (Figure 5) indicates low metal-support interactions for the HPG 700 catalyst compared with HPG900; this is suggested to be related to the higher hydrogen production of the HPG 700 catalyst. Also the higher hydrogen yield might be due to further promotion of carbon-steam reaction, which results in lower carbon deposition over the reacted catalyst, and more hydrogen released together with carbon monoxide. For comparison, Li et al [36], reported that about 54wt.% of hydrogen concentration was obtained in the produced gas, using a tri-metallic catalyst (Ni-La-Fe/Al<sub>2</sub>O<sub>3</sub>) and municipal solid waste (MSW) as raw material in a fixed bed reaction system. Higher hydrogen concentrations than 54wt.% in the product gas were attained in this work using the Ni/SiO<sub>2</sub> catalysts prepared by homogeneous precipitation and calcined at 500 and 700 °C.

For the series of BHPG catalysts, the highest catalytic activity was found for the B-HPG700 catalyst with a hydrogen production of  $19 \text{ mmol H}_2 \text{ g}^{-1}_{\text{RDF}}$ , and a gas yield of ~59 wt.% (Table 2). Using this catalyst (B-HPG700) also resulted in the lowest  $\text{CH}_4$  and  $\text{C}_2\text{-C}_4$  concentrations for this series of catalysts. Here, it is further shown that the catalyst calcined at lower temperature ( $700 \text{ }^\circ\text{C}$ ) exhibits higher hydrogen production compared with the catalyst calcined at  $900 \text{ }^\circ\text{C}$ ; this is also supported by the TPR results (Figure 5), where the catalysts calcined at  $900 \text{ }^\circ\text{C}$  show a higher reduction temperature (related to higher interactions between Ni metals species and silica support). Table 2 shows a reduction in the CO and an increase in the  $\text{CO}_2$  when using the B-HPG900 catalyst, which might indicate a promotion of the water-gas shift reaction. In addition, the B-HPG900 catalyst produced the highest concentrations of  $\text{CH}_4$  and  $\text{C}_2\text{-C}_4$ .

For all the catalysts tested, the highest activity towards methane and light hydrocarbons decomposition was achieved using the catalysts calcined at  $700 \text{ }^\circ\text{C}$ , whereas lower activity was attained using the catalysts calcined at  $900 \text{ }^\circ\text{C}$ . This might indicate a lower promotion of hydrocarbons and tar cracking reactions when using this type of catalyst calcined at temperatures higher than  $700^\circ\text{C}$ . However, the catalytic performance is also related to the catalyst properties such as surface area. For example, the surface area was reduced from 446 to  $318 \text{ m}^2 \text{ g}^{-1}$  as the calcination temperature was increased from  $700 \text{ }^\circ\text{C}$  to  $900 \text{ }^\circ\text{C}$  for the BHPG catalysts.

One relevant parameter from the BET analysis is the total surface area as it is generally related to the accessibility of active sites, hence it is associated with the catalytic activity [37]. From the results obtained it was observed that for the BHPG catalysts, the activity towards hydrogen production followed the same order as the surface area; the highest surface area of  $440 \text{ m}^2 \text{ g}^{-1}$  resulted in the highest hydrogen production  $19 \text{ mmol H}_2 \text{ g}^{-1}_{\text{RDF}}$ . From the XRD analysis (Figure 3(a)), broader peaks for the NiO crystals were observed for the

HPG700 catalyst which indicates a smaller crystal particle size when compared with those peaks for the B-HPG700 catalyst. The larger pore size and smaller crystal size, may have resulted in a better metal dispersion for the HPG700 catalyst, this was also verified by the TEM images of the fresh catalysts (Figure 4(c)). All these properties for the HPG700 catalyst may have influenced the higher hydrogen yield when compared with the other catalysts.

Lower methane and C<sub>2</sub>-C<sub>4</sub> concentrations were obtained for both series of catalysts using the catalysts calcined at 700 °C. The highest methane and C<sub>2</sub>-C<sub>4</sub> concentrations were obtained using the catalysts calcined at 900 °C for both preparation methods, indicating that catalyst properties resulting from different calcination temperatures have close relationships with their performance in the reforming process. For example, from the surface area analysis (Table 1) it was observed that the surface area of the B-HPG catalysts was drastically reduced from 446 m<sup>2</sup> g<sup>-1</sup> to 318 m<sup>2</sup> g<sup>-1</sup> when the calcination temperature was increased from 700 °C up to 900 °C. In addition, the HPG900 catalyst also exhibited the lowest surface area among the three HPG catalysts.

### 3.3 Characterization of reacted catalysts.

The reacted catalysts were analysed to identify carbon deposition over their surface, which is normally related to catalyst deactivation. From the thermogravimetric analysis (TGA-TPO), it was found that a very low amount of carbon was deposited over the catalysts after the catalytic steam reforming process. Ni crystals were formed from the catalyst reduction with H<sub>2</sub> and CO produced during the pyrolysis-reforming process; the presence of Ni particles was shown by TEM analysis (Figure 4(c), (d); Figure S4), XRD patterns (Figure 3(a)), and confirmed by SEM-EDX analysis (Figure S3).

From the SEM analysis of the BHPG's reacted catalysts, filamentous carbons were clearly observed (Figure 7(c); Figure S3(b)). Additionally, through TEM analysis (Figure 7d-

f; Figure S4), the presence of metal agglomerates for both reacted catalysts (HPG700 and B-HPG700) were observed, with a greater presence of such agglomerates for the reacted BHPG catalyst (Figure 7(e), (f)). It is suggested that catalyst sintering occurs during the reforming process; which might result in catalyst deactivation.

The DTG-TPO curves of the reacted Ni/SiO<sub>2</sub> catalysts prepared by HPG and combined HPG and phase separation methods are presented in Figure 6. For the B-HPG900 catalyst (Figure 6(a)), the initial weight decrease at around 100 °C was related to water vaporization [5], followed by significant peaks of weight increase between 400 °C and 500 °C, and associated with nickel oxidation [5,34]. From Figure 6(a) is noted that the nickel oxidation peak is shifted to lower temperatures for the B-HPG500 and B-HPG700 catalysts, as a result of the increase in the calcination temperature over the metal oxidation. However as the calcination temperature was further increased to 900 °C, this oxidation peak shifted to higher temperatures, which might indicate a major promotion of the metal oxidation.

The double peak shown for the reacted B-HPG700 catalyst between 500 °C and 600 °C (Figure 6(a)), suggests the presence of two different types of carbon deposited over the catalyst surface. It has been reported that the oxidation of amorphous carbon starts at around 500 °C, where the first peak appears, whereas the oxidation of filamentous carbon starts at around 600 °C, where the second peak appears [38,39]. The SEM image of the B-HPG900 reacted catalyst (Figure 7(c)), suggests the presence of at least two different types of carbons deposited over the reacted catalyst's surface.

The amount of carbon deposited was calculated from the weight loss of the reacted catalyst after 400 °C and this value was divided by the final weight of the catalyst after the TGA-TPO analysis [5]. For the reacted BHPG catalysts, carbon deposition was about 0.12, 0.13, and 0.11 mg g<sup>-1</sup><sub>RDF</sub> for the catalysts calcined at 500, 700 and 900 °C respectively. The similarity in the carbon deposition values for the BHPG reacted catalysts might suggest a low

influence of the carbon over the catalyst activity. Further SEM-EDX analysis allowed the identification of a carbon peak in the reacted B-HPG700 catalyst (Figure S3).

For the HPG's reacted catalysts, a different trend in the TPO curves was observed as the oxidation peaks appear at different temperatures (Figure 6(b)). Two oxidation peaks appear at around 400 °C and 700 °C, respectively, for the reacted HPG900 catalyst. The first peak suggests the presence of amorphous carbons, whereas the second endothermic peak suggests the presence of filamentous carbons. From the SEM analysis some filamentous carbons could be observed over the surface of the HPG900 catalyst (Figure 7b). The HPG500 and HPG700 catalysts showed oxidation peaks ~650 °C, which it is related to the deposition of filamentous carbon. Comparison of SEM images for the reacted HPG700 (Figure 7a) and HPG900 (Figure 7b) catalysts showed that different carbon types were observed over the reacted catalyst surface, which is in accordance with the DTG-TPO curves obtained.

#### **4. Conclusions**

In this paper, a series of Ni/SiO<sub>2</sub> catalysts were prepared using two different methods, and using different calcination temperatures. Using homogeneous precipitation based on a sol-gel method (HPG), it is possible to obtain a Ni/SiO<sub>2</sub> catalyst where the Ni was homogeneously dispersed within the silica network. The addition of the phase separation step to the simple HPG process (BHPG), resulted in an enlargement of the pores and an increase in the surface area of the final catalyst. However adding the separation step was significantly more time consuming and no improvement in the catalyst performance towards hydrogen production was attained.

An influence of the calcination temperature on both catalyst characteristics and performance was found. For example, increasing the calcination temperature from 700 to

900°C resulted in a reduction of both surface area and hydrogen concentration in the produced gas. The catalytic activities towards hydrogen production for the catalysts prepared in this work followed the order:

HPG700 > HPG500 > B-HPG700 > HPG900 > B-HPG500 > B-HPG900

The relatively low amount of carbon deposited over the catalysts surface and from the electron-microscopy analysis, suggested that the deactivation mechanism for this type of catalyst might be due to the agglomeration of metal particles (sintering), rather than through carbon deposition.

## **ACKNOWLEDGEMENTS**

The authors would like to thank the National Council of Science and Technology of Mexico (Conacyt) for the Scholarship of one of us (PHBS). Funding from the UK Science & Engineering Research Council (Grant EP/G036608/1) is also gratefully acknowledged.

## **ADDITIONAL INFORMATION**

Supporting information available: HPG and BHPG preparation methods graphic description, additional TEM images, SEM-EDX analysis, N<sub>2</sub> adsorption-desorption isotherms of fresh HPG and B-HPG samples.

**REFERENCES**

1. Haryanto A, Fernando S, Murali N, Adhikari S. Current status of hydrogen production techniques by steam reforming of ethanol: A review. *Energy Fuels* 2005;19(5):2098-2106.
2. Edwards PP, Kuznetsov VL, David WIF. Hydrogen energy. *Phil Trans Royal Soc A* 2007;365(1853):1043-1056.
3. Zhang L, Lin J, Chen Y. Studies of surface NiO species in NiO/SiO<sub>2</sub> catalysts using temperature-programmed reduction and X-ray diffraction. *J Chem Soc Faraday Trans* 1992;88(14):2075-2078.
4. Ni M, Leung DYC, Leung MKH. A review on reforming bio-ethanol for hydrogen production. *Int J Hydrogen Energy*. 2007;32 (15): 3238-3247.
5. Wu CF, Williams PT. A Novel Nano-Ni/SiO<sub>2</sub> Catalyst for Hydrogen Production from Steam Reforming of Ethanol. *Environ Sci Technol* 2010;44(15):5993-5998.
6. Takahashi R, Sato S, Sodesawa T, Suzuki M, Ichikuni N. Ni/SiO<sub>2</sub> prepared by sol-gel process using citric acid. *Micro Meso Mats* 2003;66(2-3):197-208.
7. Galuszka J, Back MH. Iron surface morphology factor in the growth of filamentous carbon. *Carbon* 1984;22(2):141-145.
8. Zheng M, Zhao T, Wu W, Li F, Yang Y. Preparation and characterization of CuO/SiO<sub>2</sub> and NiO/SiO<sub>2</sub> with bimodal pore structure by sol-gel method. *J Sol-Gel Sci Techn* 2006;39(2):151-157.
9. Goncalves G, Lenzi MK, Santos OAA, Jorge LMM. Preparation and characterization of nickel based catalysts on silica, alumina and titania obtained by sol-gel method. *J Non-Crys Solid* 2006;352:3697-3704.
10. Ermakova MA, Ermakov DY. High-loaded nickel-silica catalysts for hydrogenation, prepared by sol-gel Route: structure and catalytic behavior. *Appl Catal A Gen* 2003;245(2):277-288.
11. Nakamura N, Takahashi R, Sato S, Sodesawa T, Yoshida S. Ni/SiO<sub>2</sub> catalyst with hierarchical pore structure prepared by phase separation in sol-gel process. *Phys Chem Chem Phys* 2000;2(21):4983-4990.
12. Gil A, Diaz A, Gandia LM, Montes M. Influence of the preparation method and the nature of the support on the stability of nickel catalysts. *Appl Catal A Gen* 1994;109(2):167-179.
13. Udengaard NR. Hydrogen production by steam reforming of hydrocarbons. *Preprints of Papers - American Chemical Society, Division of Fuel Chemistry* 2004;49(2):2.
14. Satterfield CN. *Heterogenous catalysis in practice*. 2nd ed. McGraw-Hill Chemical Engineering Series. 1980, London: McGraw-Hill.
15. Tomiyama S, Takahashi R, Sato S, Sodesawa T, Yoshida S. Preparation of Ni/SiO<sub>2</sub> catalyst with high thermal stability for CO<sub>2</sub>-reforming of CH<sub>4</sub>. *Appl Catal A Gen* 2003;241(1-2):349-361.
16. Nakanishi K, Takahashi R, Nagakane T, Kitayama K, Koheiya N, Shikata H, Soga N. Formation of hierarchical pore structure in silica gel. *J Sol-Gel Sci Techn* 2000;17(3):191-210.
17. Takahashi R, Sato S, Sodesawa T, Nakamura N, Tomiyama S, Kosugi T, Yoshida S. Nanosized Ni/SiO<sub>2</sub> catalyst prepared by homogeneous precipitation in wet silica gel. *J Nanosci Nanotechn* 2001;1(2):169-176.

18. Takahashi R, Sato S, Tomiyama S, Ohashi T, Nakamura N. Pore structure control in Ni/SiO<sub>2</sub> catalysts with both macropores and mesopores. *Micropor Mesopor Mats* 2007;98(1-3):107-114.
19. Brinker CJ. Hydrolysis and condensation of silicates: Effects on structure. *J Non-Cryst Solids* 1988;100:31-50.
20. Blanco PH, Wu C, Onwudili JA, Williams PT. Characterization of tar from the pyrolysis/gasification of refuse derived fuel: Influence of process parameters and catalysis. *Energy Fuels* 2012;26(4):2107-2115.
21. Blanco PH, Wu C, Onwudili JA, Dupont V, Williams PT. Catalytic pyrolysis/gasification of refuse derived fuel for hydrogen production and tar reduction: Influence of nickel to citric acid ratio using Ni/SiO<sub>2</sub> catalysts. *Waste Biomass Valoriz* 2013;(In Press).
22. Blanco PH, Wu C, Onwudili JA, Williams PT. Characterization and evaluation of Ni/SiO<sub>2</sub> catalysts for hydrogen production and tar reduction from catalytic steam pyrolysis-reforming of refuse derived fuel. *Appl Catal B Environ* 2013;134:238-250.
23. Buah WK, Cunliffe AM, Williams PT. Characterization of products from the pyrolysis of municipal solid waste. *Proc Safe Environ Protect* 2007;85(5):450-457.
24. Brunauer S, Emmett PH, Teller E. Adsorption of gases in multimolecular layers. *J Am Chem Soc* 1938;60(2):309-319.
25. Barrett EP, Joyner LG, Halenda PP. The determination of pore volume and area distributions in porous substances. I. Computations from nitrogen isotherms. *J Am Chem Soc* 1951;73(1):373-380.
26. Parr RG, Yang W. Density-functional theory of atoms and molecules, O.S. Publications. 1989, Oxford: Clarendon Press.
27. Olivier JP. Improving the models used for calculating the size distribution of micropore volume of activated carbons from adsorption data. *Carbon*, 1998;36(10):1469-1472.
28. Ermakova MA, Ermakov DY. Ni/SiO<sub>2</sub> and Fe/SiO<sub>2</sub> catalysts for production of hydrogen and filamentous carbon via methane decomposition. *Catal Today* 2002;77(3):225-235.
29. Sing KSW, Everett DH, Haul RAW, Moscou L, Pierotti RA, Rouquerol J, Siemieniewska T. Reporting Physisorption Data for Gas Solid Systems with Special Reference to the Determination of Surface-Area and Porosity (Recommendations 1984). *Pure Appl Chem* 1985;57(4):603-619.
30. Neimark AV, Ravikovitch PI, Vishnyakov A. Adsorption hysteresis in nanopores. *Phys Rev E* 2000;62(2):R1493-R1496.
31. Ravikovitch PI, Neimark AV. Characterization of micro- and mesoporosity in SBA-15 materials from adsorption data by the NLDFT method. *J. Phys. Chem. B*, 2001;105(29):6817-6823.
32. Rouquerol F, Rouquerol J, Sing KSW. *Adsorption by Powders and Porous Solids*. 1999, London: Academic Press.
33. Cho YS, Park JC, Lee B, Kim Y, Yi J. Preparation of mesoporous catalyst supported on silica with finely dispersed Ni particles. *Catal Lett* 2002;81(1-2):89-96.
34. Wu CF, Wang L, Williams PT, Shi J, Huang J. Hydrogen production from biomass gasification with Ni/MCM-41 catalysts: Influence of Ni content. *Appl Catal B Environ* 2011;108(1-2):6-13.
35. Sookman C, Kongkachuichay P, Tanakulrungsank W. The effect of calcined temperature on the property of nickel oxide catalyst synthesized by sol-gel method,

- In, International symposium Eco-Energy and Material Science and Engineering Symposium. 2005, EMSES: Chiangmai, Thailand.
36. Li J, Liu J, Liao S, Zhou X, Yan R. Syn-Gas Production from Catalytic Steam Gasification of Municipal Solid Wastes in a Combined Fixed Bed Reactor. *Int Conf Intell Syst Design & Eng App* 2010, 530-534.
  37. Kim P, Kim Y, Kang T, Song IK, Yi J. Preparation of nickel-mesoporous materials and their application to the hydrodechlorination of chlorinated organic compounds. *Catal Surveys Asia* 2007;11(1):49-58.
  38. Wu C, Williams PT. Hydrogen production by steam gasification of polypropylene with various nickel catalysts. *Appl Catal B Environ* 2009;87(3-4):152-161.
  39. Wu C, Williams PT. Investigation of coke formation on Ni-Mg-Al catalyst for hydrogen production from the catalytic steam pyrolysis-gasification of polypropylene. *Appl Catal B Environ* 2010;96(1-2):198-207.

Table 1. Surface and porous properties of fresh Ni/SiO<sub>2</sub> catalysts

Catalyst	Ni content (wt%)	Surface area <sup>1</sup> (m <sup>2</sup> g <sup>-1</sup> )	Micropore volume <sup>2</sup> (cm <sup>3</sup> g <sup>-1</sup> )	Mesoporous volume <sup>2</sup> (cm <sup>3</sup> g <sup>-1</sup> )	Pore diameter <sup>3</sup> (nm)	Average Mesopore Size (nm) <sup>4</sup>
HPG500	10	363	0.18	0.86	9.76	7.45
HPG700	10	347	0.18	0.91	12.50	8.92
HPG900	10	313	0.16	0.84	9.75	7.45
B-HPG500	10	387	0.22	0.80	12.58	8.92
B-HPG700	10	446	0.25	0.92	9.46	7.45
B-HPG900	10	318	0.16	0.82	12.63	11.17

<sup>1</sup> MultiPoint Brunauer, Emmett & Teller (BET) Method

<sup>2</sup> Dubinin-Radushkevich (DR) Method

<sup>3</sup> Barrett, Joyner & Halenda (BJH) Method

<sup>4</sup> Density Functional Theory (DFT)

Table 2. Gas composition and mass balance of pyrolysis-reforming products

Catalyst	Gas composition (Vol.%, N <sub>2</sub> free)					Hydrogen production (mmol H <sub>2</sub> g <sup>-1</sup> RDF)	Gas yield (wt.%)	Char/RDF (wt.%)	Mass Balance (wt.%)
	CO	H <sub>2</sub>	CO <sub>2</sub>	CH <sub>4</sub>	C <sub>2</sub> -C <sub>4</sub>				
HPG500	22.4	55.3	17.2	3.8	1.3	18.5	53.2	29.4	96.2
HPG700	23.5	59.3	13.9	2.8	0.6	21.5	52.6	29.4	92.9
HPG900	23.3	52.0	17.3	5.3	2.1	14.4	46.2	28.9	90.8
B-HPG500	25.8	49.7	17.5	5.4	1.6	16.8	58.2	30.0	94.9
B-HPG700	28.0	53.4	14.7	3.1	0.7	19.4	58.6	29.2	95.7
B-HPG900	24.6	42.3	16.8	11.0	5.3	9.7	42.4	28.8	92.5

**FIGURE CAPTIONS**

Figure 1. Adsorption-desorption isotherms for selected prepared catalysts

Figure 2. Pore size distribution (DFT): 2(a) HPG, and 2(b) B-HPG Ni/SiO<sub>2</sub> catalysts

Figure 3. Analysis of selected Ni/ SiO<sub>2</sub> samples: 3(a) XRD analysis; and 3(b) IR spectra

Figure 4. Fresh catalysts morphology; SEM images: (a) HPG700; (b) B-HPG700; TEM images: (c) HPG700; (d) B-HPG700

Figure 5. Temperature programme reduction (TPR) of the fresh catalysts

Figure 6. Thermogravimetric analysis of reacted catalysts DTG-TPO curves: 5(a) BHPG, and 5(b) HPG catalysts

Figure 7. Images of reacted catalysts; SEM: (a) HPG700; (b) HPG900; (c) B-HPG900; TEM: (d) HPG700; (e) B-HPG700; (f) B-HPG700

Figure 1. Adsorption-desorption isotherms for selected prepared catalysts

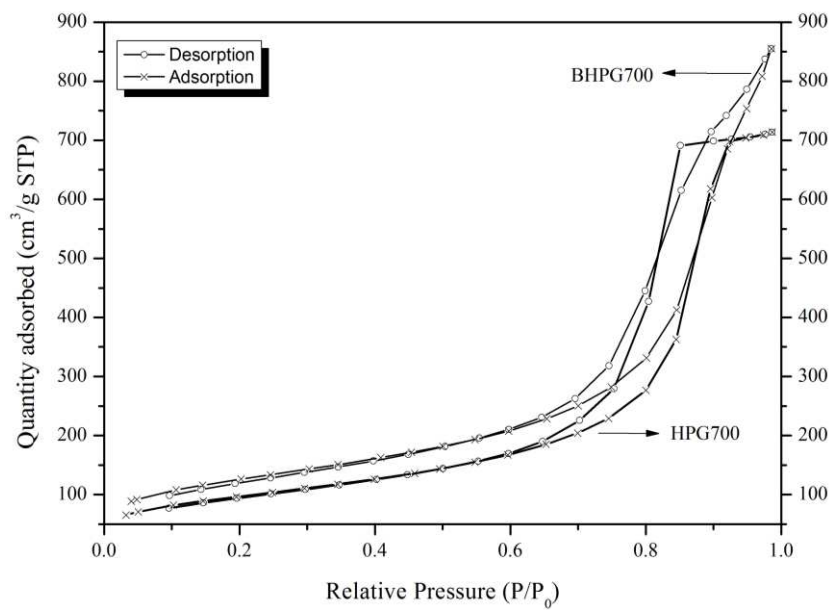


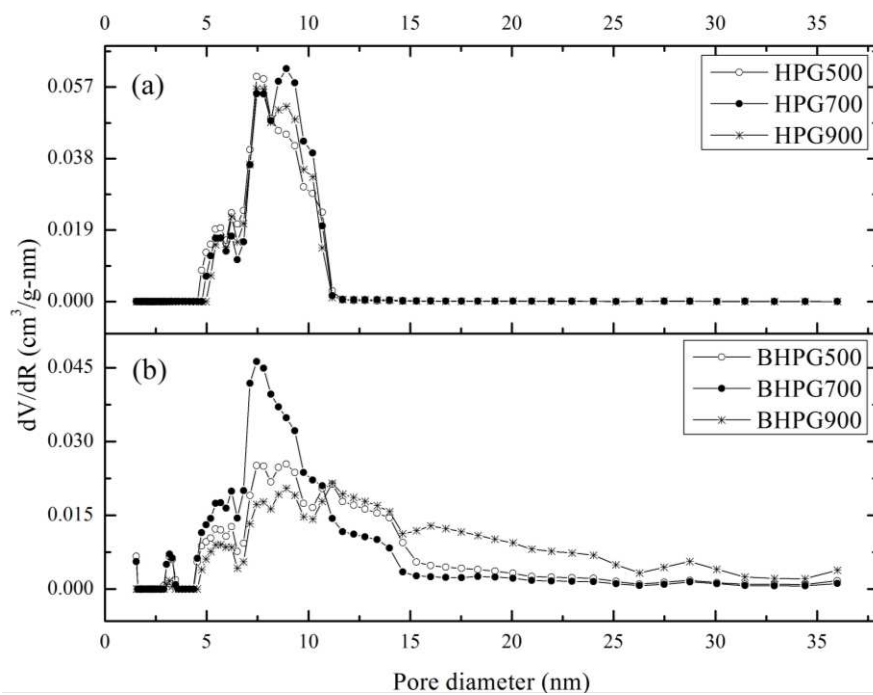
Figure 2. Pore size distribution (DFT): 2(a) HPG, and 2(b) B-HPG Ni/SiO<sub>2</sub> catalysts

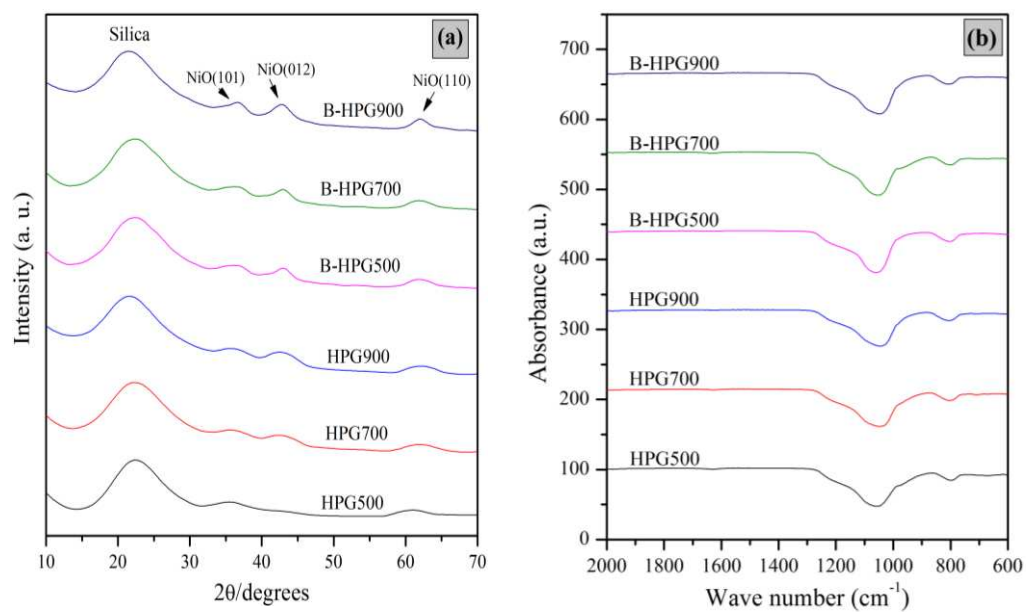
Figure 3. Analysis of selected Ni/ SiO<sub>2</sub> samples: 3(a) XRD analysis; and 3(b) IR spectra.

Figure 4. Fresh catalysts morphology; SEM images: (a) HPG700; (b) B-HPG700; TEM images: (c) HPG700; (d) B-HPG700

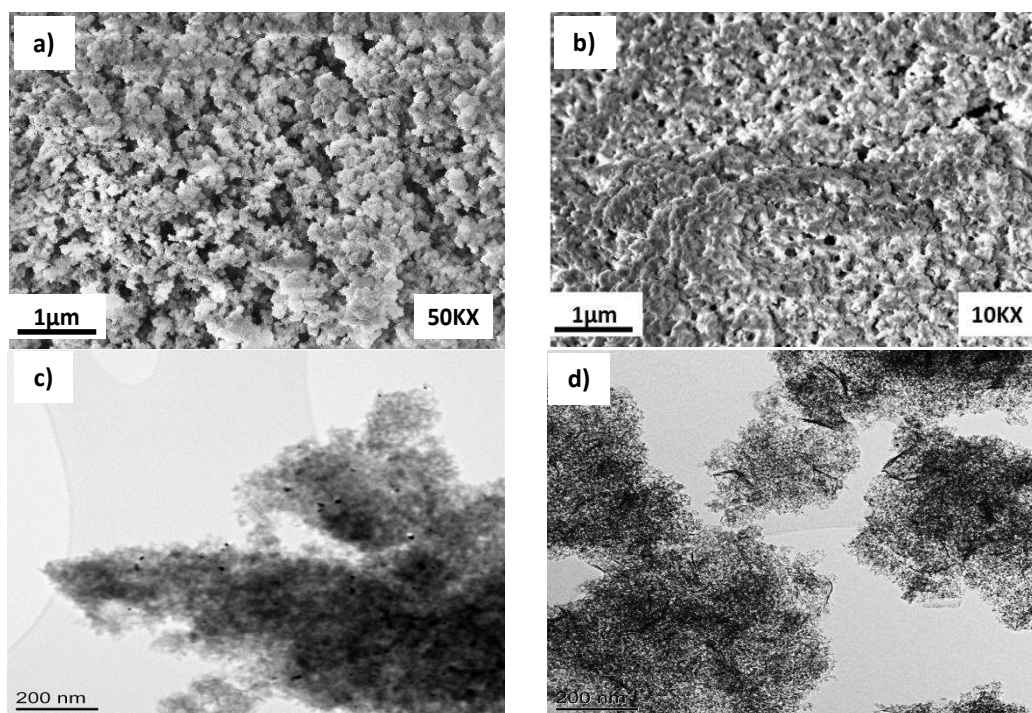


Figure 5. Temperature programme reduction (TPR) of the fresh catalysts

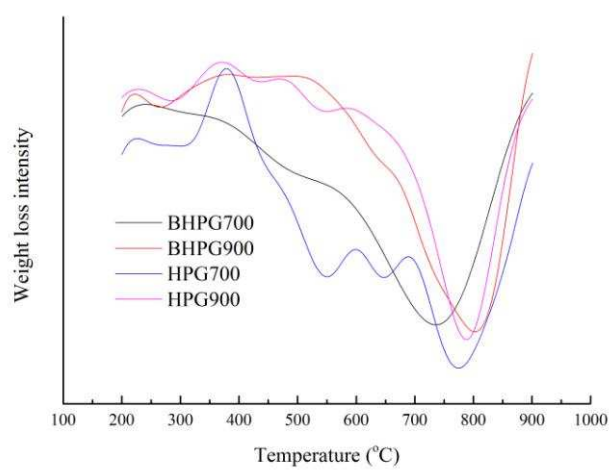


Figure 6. Thermogravimetric analysis of reacted catalysts DTG-TPO curves: 5(a) BHPG, and 5(b) HPG catalysts

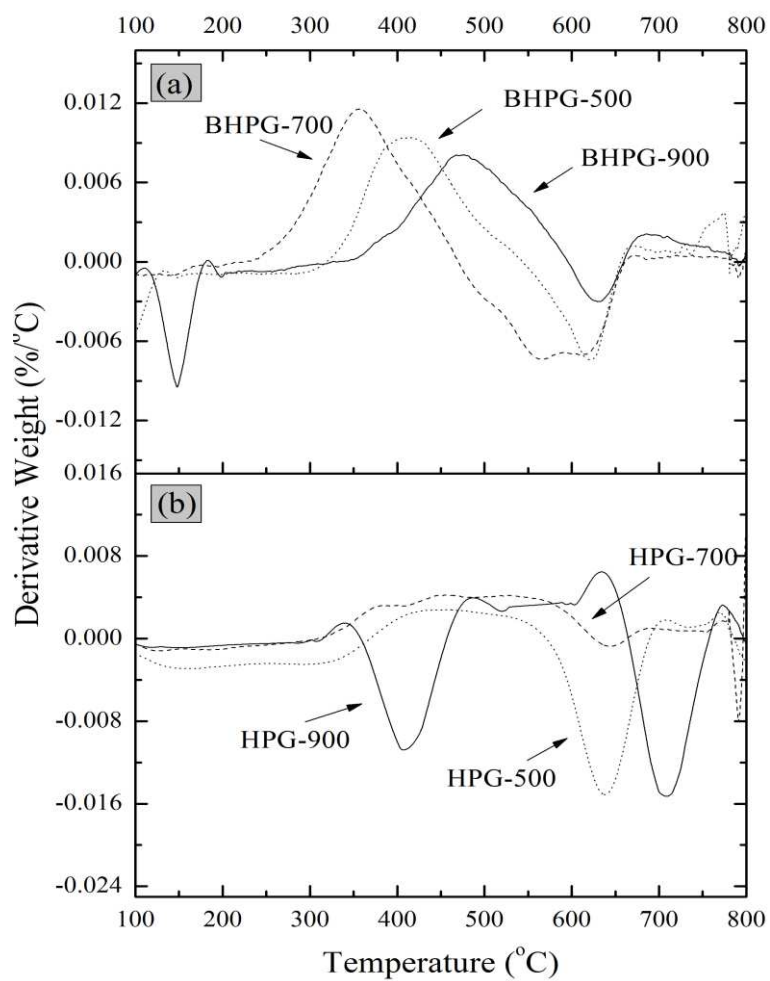


Figure 7. Images of reacted catalysts; SEM: (a) HPG700; (b) HPG900; (c) B-HPG900; TEM: (d) HPG700; (e) B-HPG700; (f) B-HPG700

